Estimation of Impulsive Noise in an Electricity Substation

Qingshan Shan, *Member, IEEE*, Ian A. Glover, *Member, IEEE*, Robert C Atkinson, *Senior Member, IEEE*, Shahzad A Bhatti, *Member, IEEE*, Iliana E Portugues, *Member, IEEE,* Philip J Moore, *Senior Member, IEEE*, Richard Rutherford, Maria Fatima Q Vieira, Antonio Marcus N. Lima, *Member, IEEE*, and Benemar Alencar de Souza, *Senior Member, IEEE*

***Abstract*—Measurements of impulsive noise in a 400/275/132 kV electricity substation are presented. The measurements are made with three antennas having overlapping bands covering the range 100 MHz to 6 GHz. This range includes those bands relevant to modern wireless local area network, and wireless personal area network, technologies (e.g. IEEE 802.11a/b/g and IEEE 802.15.1/4) which, if proved to be sufficiently robust in the presence on impulsive noise, could play a useful role in substation monitoring and control. Impulsive events are extracted from the measured data using the wavelet packet transform and the statistical distributions of pulse rate, pulse amplitude, pulse duration, and pulse rise-time are presented. An unexpected quasi-periodic component of the noise is observed.**

***Index Terms*— Bluetooth, electricity substations, impulsive noise, noise amplitude distribution, partial discharge, wireless local area network, ZigBee.**

I. Introduction

IMPULSIVE noise has the potential to degrade the performance and reliability of wireless communications systems [1]. Such noise, which is especially prevalent in high-voltage electricity substations, has discouraged the deployment of wireless technologies for operational purposes in the electricity supply industry (ESI). A model of impulsive noise specific to electricity substations would allow the assessment of risk associated with such deployment for monitoring and control functions. Much effort has already been devoted to the measurement of impulsive noise in a variety of physical environments, spanning various frequency bands, with a view to assessing its impact on a range of wireless communication technologies. The environments include urban, rural, industrial, medical, and commercial [1-4]. The bands lie between 40 MHz and 4 GHz and the communication technologies include satellite-mobile, digital TV, and the universal mobile telecommunications system [2, 5-6]. In all these campaigns the measurement bandwidths have been relatively narrow, ranging from 120 kHz to 40 MHz.

In this collaborative paper we present wideband measurements of impulsive noise in the specific environment of a 400/275/132 kV air-insulated substation. Such data is required to assess the impact of this environment on the performance of modern wireless technologies operating in frequency bands up to 6 GHz including WiFi (and other wireless local area network (WLAN) systems), Bluetooth and ZigBee. The operating frequencies of these technologies, as defined by IEEE standards 802.11a/b/g [7], 802.15.1 [8] and 802.15.4 [9], respectively, are listed in Table I. The authors are not aware of any existing measurements that can be used to assess the resilience of these modern wireless technologies to the particular impulsive noise environment found in substations.

Within electricity substations, impulsive noise could occur due to partial discharge (PD), periodic processes from power electronic and other equipment, and lower-frequency, sporadic, events due to switching. The emphasis in this study, however, is on the aggregate impulsive noise background irrespective of its physical origin. Whilst impulsive noise power may be relatively strong close to its source, it decays rapidly with distance [10]. (Since impulsive noise is rarely radiated intentionally both its absolute power and the gain of its radiating structure are generally small. It is an assumption, therefore, that the impulsive process(es), recorded and reported here, originate within the substation compound.) To characterize it properly may thus require its extraction from a

TABLE I
FREQUENCY BANDS SPECIFIED BY IEEE STANDARDS

802.11a (GHz)	**802.11b/g (GHz)**	**802.15.1 (GHz)**	**802.15.4 (GHz)**
5.15 - 5.25	2.4 – 2.4835	2.4 – 2.4835	0.868 – 0.8686
5.25 - 5.35			2.4 – 2.4835
5.47 - 5.725	2.471 – 2.497 (Japan)		0.902 – 0.928 (USA)
5.725 - 5.825			

Manuscript received July 8, 2009. This work was supported by The UK Engineering & Physical Sciences Research Council (EPSRC) under Grant EP/D049687/1.

Qingshan Shan, Ian Glover, Robert Atkinson and Shahzad Bhatti are with the Centre for Excellence in Signal and Image Processing, Department of Electronic & Electrical Engineering, University of Strathclyde, Glasgow, G1 1XW, UK (phone: +44-141-5482663; fax: +44-141-5524968; e-mail: {qingshan.shan; ian.glover; r.atkinson and shahzad.bhatti}@ eee.strath.ac.uk).

Iliana Portugues and Philip Moore are with Elimpus Ltd, 28 Wren Court, Strathclyde Business Park, Bellshill, Lanarkshire ML4 3NQ, UK (E-mail: i.portugues@elimpus.com)

Richard Rutherford is with Scottish Power – Energy, Networks & Telecommunications, 1 Atlantic Quay, Glasgow, G2 8SP, UK (e-mail: Richard.Rutherford@sppowersystems.com).

Fatima Vieira, Antonio Lima and Benemar de Souza are with the Departamento de Engenharia Eletrica, Universidade Federal de Campina Grande, Campina Grande, Brazil (email: {fatima; benemar; amnlima}@ dee.ufcg.edu.br).

mixture of other unwanted signals and noise processes including coherent interference (e.g. broadcast and other communications and radar signals). This makes practical site-characterization difficult since impulsive noise sources may be significant distances from buildings where measurement equipment can be protected against environmental effects (in particular humidity and ingress of water). An effective method of extracting impulsive noise from a background of higher-power noise and interference is therefore needed. Several methods of extracting PD from other noise processes have been investigated [11] and the wavelet transform has been identified as being particularly useful [12]. The wavelet packet transform (WPT) [13], which represents a generalization of the wavelet transform, has been applied for online detection of PD in 11 kV cables [14] and used, in conjunction with neural networks, to separate corona from PD [15]. Before describing this signal processing algorithm in detail (Section IV) the noise measurement system (Section II) and the measurement campaign (Section III) are described. The statistical characteristics of the measured data are presented in Section V followed by some observations and discussion in Section VI. Since the measured variance of amplitude distribution depends on the distance to the impulsive noise source, the particular numerical value measured may not in itself be significant. Conclusions are drawn in Section VII. Section II is based on an earlier conference paper [16] of three of the authors.

II. Measurement System

An ultra-wideband detection system has been developed specifically for the monitoring and recording of impulsive noise. Since the potential interfering effects of impulsive noise will depend not only on power spectral density but also on the time-domain waveform, it is important that generic measurements should, as far as possible, retain pulse shape information, thereby allowing the effects of arbitrary filtering (introduced by commercial receivers) to be properly emulated when assessing performance impact. In view of this the measurement system has been designed not only to have wide bandwidth but also to have good (i.e. short-duration) impulse response. A block diagram of the measurement system is shown in Fig. 1. It comprises three antennas, a LeCroy SDA9000 4-channel digital storage oscilloscope (DSO), an external 1 TB hard disk drive (HDD) and a laptop computer (not shown) for data logging and data pre-processing. The DSO sampling rate is 20 GS/s per channel and its analog channel bandwidth is 6 GHz. The antennas are connected directly to the DSO. Direct sampling is used since previous studies, e.g. [17], have shown this to be advantageous in terms of minimizing signal distortion. Interconnection is with 18 GHz, 50 Ω, coaxial cables. No artificial band limiting of the antenna signals has been attempted. Measured pulses with rise-times greater than (say) 10 times the reciprocal of the antenna bandwidths should not, therefore, suffer significant distortion. (A consequence of not using band limiting filters is that the recorded signals will not be orthogonal.) Time-series are recorded using conventional amplitude triggering. Each recorded time-series is 2.5 ms in duration which is the longest possible using the available DSO RAM. The recorded signals are saved to the external HDD which is connected to the DSO via a USB interface.

Two quasi-TEM half-horns, a high-band (HB) horn and low-band (LB) horn, have been designed to cover the previously unexplored frequency range above 700 MHz. Quasi-TEM horns were selected for the frequency bands of greatest (most novel) interest due to their wide bandwidth, linear phase response and, thus, excellent impulse characteristics. Two horn antennas were used since a single antenna covering the entire band was found to be impractical without compromising the phase characteristic. The LB horn covers the range 0.7 – 2 GHz and the HB horn covers the range 2 – 6 GHz.

The third antenna is a discone [16] used to extend data collection below 700 MHz (i.e. into the bands already investigated in the context of PD).

The TEM horn, in its basic form, consists of two isosceles conducting plates. The apexes of the plates (i.e. the corners with smallest angle) form the antenna feed-point. The sides of each plate opposite the apex are parallel and form the antenna aperture. The flare angle (the angle between the planes of the plates), apex angle and plate length are chosen such that the characteristic impedance at the feed-point is equal to that of the feeding transmission line and the impedance at the aperture is equal to the plane-wave impedance of free space. The three principal design parameters, Fig. 2(a), are the length of antenna, L (measured perpendicularly from aperture to feed point), the azimuth angle of the antenna plates, α, and the flare angle between the antenna plates, β. L, which determines the lower end of the antenna frequency response, must be at least one half-wavelength at the lowest frequency of interest. The upper end of the frequency response is inversely proportional to the separation between the plates at the feed point.

The TEM half-horn comprises a single triangular plate mounted above a ground plane. Details of the half-horn designs were reported in [18]. A summary is included below, however, along with the discone antenna.

LB Horn

The LB horn is constructed from a triangular aluminum plate and a 122 cm × 122 cm aluminum ground plane. The width (w) of the triangular plate at the aperture is 65.1 cm, its length (L) is 84 cm, and its aperture height measured from the ground plane (h) is 20.1 cm. The antenna feed is a 50 Ω SMA connector with its flange in electrical contact with the ground plane and its center-conductor connected to the triangular plate apex. The amplitude response, measured using a network analyzer, shows the 3dB bandwidth of a pair of identical cascaded horns (transmit and receive) to be 1.264 GHz covering the frequency range 716 MHz - 1.98 GHz. The peak value of the amplitude response occurs at 1.068 GHz.

HB Horn

The HB horn triangular flange is constructed from a printed circuit board. The flange width (w) at the aperture is 21.7 cm and its length (L) is 28 cm. The aperture height (h) is 6.7 cm. The feed structure and ground plane are identical to those of

the LB horn. The 3dB bandwidth of a cascaded pair (transmit and receive) is 3.195 GHz (1.905 to 5.1 GHz) and the peak value of the amplitude response occurs at 2.13 GHz.

Discone Antenna

The discone antenna covers frequencies below about 700 MHz. This is the frequency range conventionally assumed to be important for PD. The details of this antenna design were reported in [16]. A schematic diagram is shown in Fig. 2(b).

The discone antenna consists of an inverted right circular cone over a circular ground plane. The ground plane is 17.1 cm in diameter and is constructed from aluminum plate. The cone was machined from solid aluminum. It has a base diameter of 13.3 cm and a height of 5.4 cm. A non-inverted cone with equal base diameter sits on top of the inverted cone. Its height is 4.9 cm. This antenna was designed and constructed as part of a previous project [19] and has not had its bandwidth characterized in the same way as the TEM horns. Its measured s-parameter, S11, indicates a -6 dB upper frequency close to 700 MHz, however, and an impedance bandwidth in excess of 0.6 GHz.

III. Measurement Campaign

The measurement site is Strathaven 400/275/132 kV air-insulated substation in the UK, owned by Scottish Power Ltd.

Fig. 3(a) shows the system deployed in the 400 kV substation control room. All antennas were deployed with vertical polarization. Figs. 3(b), (c) and (d) show composite images of the 400 kV, 275 kV and 132 kV compounds, respectively. The 400 kV and 275 kV control rooms, in which the measurement system has been deployed, are shown on the left in Figs. 3(b) and (c). The control rooms are located close to the center of the substation compound, Fig. 4. The substation is itself located in a rural area.

TABLE II(A)
PARAMETERS OF BEST-FIT DISTRIBUTIONS

Process	Antenna	Distribution	Parameter	
Impulse rate	Discone	Generalized Extreme Value	μ	1.14×10^{5} s^{-1}
			σ	1.52×10^{4} s^{-1}
			l	1.07×10^{5} s^{-1}
			s	9.92×10^{3} s^{-1}
			ν	1.15×10^{-1}
	LB horn	Generalized Extreme Value	μ	1.27×10^{5} s^{-1}
			σ	6.61×10^{4} s^{-1}
			l	9.75×10^{4} s^{-1}
			s	3.75×10^{4} s^{-1}
			ν	1.84×10^{-1}
	HB horn	Generalized Extreme Value	μ	1.17×10^{5} s^{-1}
			σ	1.81×10^{4} s^{-1}
			l	1.08×10^{5} s^{-1}
			s	1.06×10^{4} s^{-1}
			ν	1.71×10^{-1}
Impulse amplitude	Discone	Gaussian (Normal)	μ	1.95×10^{-1} mV
			σ	0.537 mV
	LB horn	Gaussian (Normal)	μ	-4.22×10^{-2} mV
			σ	0.905 mV
	HB horn	Gaussian (Normal)	μ	-1.46×10^{-1} mV
			σ	0.454 mV

μ - mean value; σ – standard deviation; l - location; s - scale; ν - shape

IV. Data Processing

An example of raw data recorded in the substation is shown in Fig. 5(a). The abscissa represents sampling time (in μs) and the ordinate represents signal level (in mV).

Two stages of data processing are employed to extract impulsive events. The first stage separates impulsive 'signals' from non-impulsive 'noise' using wavelet-based analysis. We refer to this as 'de-noising'. Positive or negative pulses can result from this analysis since the wavelet algorithm is analogous to correlating the raw data with a synchronized reference signal of optimum scale and location. (This is similar to a coherent detection process using a reference signal which may be either phase aligned with, or phase opposed to, the signal being received.) The second stage extracts the pulse parameters (rate, amplitude, duration, and rise-time) from the de-noised data.

Each time-series record of 50 Msamples is divided into five data-blocks containing 10 Msamples prior to processing.

A. De-noising

Wavelet packet transformation is central to the extraction of impulses from the Strathaven measurement database [20]. The signal pre-processing involves four steps. These are:

1) *Decomposition of both approximation and detail*: The choice of decomposition level was based on the available computer resources (CPU 2.33GHz, 1GB RAM) and the number of samples to be processed[1]. The symlet-6 wavelet was used as shown in Fig. 6.
2) *Computation of best tree*: The optimal wavelet packet tree is computed with Stein's unbiased risk estimate (SURE) entropy function.
3) *Wavelet-packet coefficient thresholding*: Hard thresholding is applied to the coefficients of each packet.
4) *Reconstruction*: The required signal is reconstructed based on the original approximation coefficients at each level and the modified detail coefficients.

The de-noised data corresponding to the raw measurement of Fig. 5(a) is shown in Fig. 5(b).

B. Feature Extraction

The algorithm developed in this study comprises the following six steps:

1) *Calculation of threshold value*: The threshold value, T, is the lesser of T_1 and T_2 given by

[1]Each data-block of 10 Msamples was divided into data-segments containing 200,020 samples (or fewer) prior to processing. A data-segment with 200,020 samples can be decomposed using up to 14 levels. At each decomposition level the data is down-sampled by a factor of two. The minimum number of samples that can be decomposed to the lowest level is therefore $2^2 = 4$. For a data-segment with 200,020 samples the maximum decomposition level is thus 17-3 = 14 ($2^{17} < 200{,}020 < 2^{18}$). For 14 levels the computation would take 28 hours to extract the impulsive noise component from a single 2.5ms (50 Msample) time-series. Decomposition with 12 levels takes less than 3 hours to process a time-series.

$$T_1 = \frac{1}{k}\max\left|X_j - \frac{\sum_{i=1}^{N} X_i}{N}\right| \quad (1)$$

and

$$T_2 = \frac{l}{N}\sum_{j=1}^{N}\left|X_j - \frac{\sum_{i=1}^{N} X_i}{N}\right| \quad (2)$$

where X is the de-noised time-series and N is the number of time-series samples. T_1 is thus $1/k$ of the maximum (unsigned) difference between any sample in the time-series and the time-series mean and T_2 is l times the mean (unsigned) difference. k (= 4) and l (= 6) were determined empirically from simulations using an artificially generated impulsive random process buried in a non-impulsive noise background. The adopted values were those that minimized the error in the number of extracted impulses.

2) *Identification of time index clusters*: A cluster is identified as a set of contiguous data points with magnitude greater than the threshold T, i.e. satisfying $|M_j| > T$ where M_j is given by

$$M_j = X_j - \frac{\sum_{i=1}^{N} X_i}{N} \quad (3)$$

The values of X_j corresponding to one time index cluster are assumed to represent one impulse.

3) *Extraction of impulse amplitude*: Impulse amplitude is the maximum value of X_j within a given time index cluster.
4) *Calculation of impulse duration*: Impulse duration is the difference of time indices corresponding to locations on either side of the maximum value that are $1/\sqrt{2}$ of the maximum value.
5) *Calculation of impulse rise-time*: Rise-time is the difference of time indices corresponding to 10% and 90% of the pulse's maximum amplitude.
6) *Calculation of mean impulse rate:* Mean impulse rate is calculated with an integration time of 2.5 ms coinciding with the length of the time-series record.

The impulse features are illustrated in Fig. 7, which is a time-dilated segment of Fig. 5(b).

500 GB of data have been processed using the above de-noising and feature extraction algorithms. The external origin of the recorded impulsive noise has been confirmed by noting that no impulses are recorded when the antennas are disconnected.

V. Results

Probability density functions (PDFs), exceedance curves (ECs), and noise amplitude distributions (NADs) have been variously calculated for the extracted impulsive noise features.

A. PDFs and ECs

PDFs and ECs of mean impulse rate, impulse amplitude, impulse duration, and impulse rise-time, have been calculated for data derived from de-noised data instances recorded using each of the antennas.

The data histograms with corresponding empirical distributions are shown in Figs. 8 – 10. The distributions have been adopted on the basis of subjective best-fit to a range of widely used functions, i.e. beta [21], binomial, Birnbaum-Saunders [22], exponential, extreme value [23], gamma, generalized extreme value [24], generalized pareto [25], inverse Gaussian [26], log-logistic [27], logistic [28], lognormal, Nakagami [29], negative binomial, normal, Poisson, Rayleigh, Rician, t location-scale, and Weibull [30]. No attempt has been made to select the distributions on the basis of physical modeling of the impulsive processes. Tables II(A) and (B) contain the parameters of the best-fit distributions.

TABLE II(B)
PARAMETERS OF BEST-FIT DISTRIBUTIONS (CONT.)

Process	Antenna	Distribution	Parameter	
Impulse duration	Discone	Generalized Extreme Value	μ	7.34×10^{1} ns
			σ	1.29×10^{2} ns
			l	4.41×10^{1} ns
			s	2.12×10^{1} ns
			ν	4.54×10^{-1}
	LB horn	Birnbaum-Saunders	μ	1.14×10^{2} ns
			σ	9.76×10^{1} ns
			s	8.45×10^{1} ns
			ν	8.40×10^{-1}
	HB horn	Birnbaum-Saunders	μ	8.05×10^{1} ns
			σ	6.03×10^{1} ns
			s	6.34×10^{1} ns
			ν	7.35×10^{-1}
Impulse rise-time	Discone	t location-scale	l	9.70×10^{1} ns
			s	1.64×10^{1} ns
			ν	9.74×10^{-1}
	LB horn	t location-scale	l	1.12×10^{2} ns
			s	3.20×10^{1} ns
			ν	1.90×10^{0}
	HB horn	t location-scale	l	9.80×10^{1} ns
			s	1.79×10^{1} ns
			ν	9.57×10^{-1}

μ - mean value; σ – standard deviation; l - location; s - scale; ν - shape

The resulting ECs are shown in Figs. 11 – 14. The 50%, 1% and 0.01% exceedance values for each antenna are given in Table III.

TABLE III
SELECTED EXCEEDANCE VALUES

Process	Antenna	50%	1%	0.01% (*0.3%)
Impulse rate (s^{-1})	Discone	109600	160800	166800
	LB horn	113600	340800	399600
	HB horn	112800	172800	183600
Impulse Amplitude (mV)	Discone	0.181	1.389	3.424
	LB horn	-0.050	3.254	10.110
	HB horn	-0.157	0.905	1.500
Impulse duration (ns)	Discone	44.85	328.95	776.3
	LB horn	78.80	320.60	593.30
	HB horn	44.95	332.75	801.60
Impulse rise-time (ns)	Discone	96.55	858.15	1832.3
	LB horn	109.35	453.00	993.05
	HB horn	96.95	866.30	1789.5

* 0.3% is used for impulse rate probability distributions

B. NADs

NAD characterization of impulsive noise retains joint information about noise impulse occurrence rate and strength [2, 31]. The ordinate of a NAD curve shows the noise impulse spectral amplitude (typically in decibels above 1 μV/MHz) and the abscissa indicates (usually on a logarithmic scale) the average number of impulses per second that exceed each of the spectral amplitude levels. The (one-sided) voltage spectral amplitude of an impulse envelope in V/Hz is given by $Q = 2A$ where A is the strength (i.e. area) of the envelope measured in Vs. For example, an impulse of 60 dB μV/MHz is equivalent to 10^3 μV/MHz or 10^{-9} V/Hz. This corresponds to an impulse strength of 5×10^{-10} Vs. The shaded area in Fig. 15 illustrates impulse strength.

A NAD analysis of the extracted feature data has been undertaken. The resulting curves are shown in Fig. 16. The average impulse rates corresponding to exceedance values of 65, 60, 50, and 40 dBμV/MHz for each antenna are given in Table IV.

TABLE IV
AVERAGE IMPULSE RATE (s^{-1}) EXCEEDED

NAD (dBμV/MHz) / Antenna	65	60	50	40
Discone	13.79	278.2	6682	39650
LB horn	101	270.2	15550	77770
HB horn	7.47	108.6	5838	35390

VI. OBSERVATIONS AND DISCUSSION

Measurement of impulsive noise in a single substation cannot be assumed to adequately represent the range of conditions that might exist across substations generally and more measurements for a range of different substation types and environments are therefore required. Nevertheless the following observations are made with respect to the measurements reported.

Impulse rate (Figs. 8(a), 9(a), 10(a)) is well-approximated by a generalized extreme value distribution, i.e.:

$$f(r|v,l,s) = \frac{1}{s}\left(1 + v\frac{(r-l)}{s}\right)^{-\frac{1}{v}} \exp\left(-\left(1 + v\frac{(r-l)}{s}\right)^{-\frac{1}{v}}\right) \quad (4)$$

where v, l, and s are shape, location and scale parameters respectively. The mean, shape, location and scale values, are similar for all three antennas and the distributions are all peaked around 10^5 Hz, with relatively narrow spread. The standard deviation of the LB horn distribution, however, is approximately four times that of the other two antennas. The peak value and relatively narrow width of the distributions is consistent with a strong component having 10 μs periodicity. This is apparent in Fig. 5(b) and has been confirmed by calculating the distribution of inter-pulse interval. This component is therefore almost certainly not PD origin and may represent conventional electromagnetic interference of electronic circuit origin. Because the measurement system was located far from the substation boundary it seems unlikely that this interference originates outside the substation. The similarity of the distributions measured by each of the three antennas suggests that that the same fundamental process(es) dominate in all three sets of data. The greater variation of impulse rate received by the LB horn suggests, however, that this antenna receives at least one process not received (or received less strongly) by the discone or HB horn. The extreme value distribution is normally used to model the smallest or largest values in a large set of independent, identically distributed, random variables. It is not obvious why the measured impulse rate should be so distributed.

Impulse amplitude (Figs. 8(b), 9(b), 10(b) and Table II(A)) is nearly symmetrically distributed about a value close to zero for all three antennas indicating approximate symmetry between positive and negative pulse processes. There is some suggestion of bimodality, however, with a notch in the pdf close to 0 V. In the case of the discone and HB horn antennas this suggestion is weak and could be an artifact of statistical noise. The suggestion is more pronounced in the case of the LB horn and a Gaussian distribution fits this data less well than the data from the discone and HB horn. This notch is not due to small amplitude impulses failing to trigger the oscilloscope since all impulse amplitudes are small with respect to the other processes in which they are immersed. The oscilloscope was therefore triggered by these larger amplitude processes (i.e. effectively randomly, or continually, depending on the precise level of the non-impulsive processes). A process subject to a minimum energy condition, such as a discharge, might be proposed to explain the missing small-amplitude pulses. That the notch is not complete (i.e. is not represented by an empty bin) could be explained by one or more additional impulsive process constrained by a similar minimum energy condition but located at greater distance, or by one or more impulsive sources of different type unconstrained by minimum energy. Such an interpretation remains speculative, however. The standard deviation for the LB horn data is approximately twice that of the other two antennas again suggesting that this antenna (and by

implication the frequency band to which it is most sensitive) is subject to a distinct impulsive process not experienced to the same extent by the other two antennas.

Impulse duration (Figs. 8(c), 9(c), 10(c) and Table II(B)) shows distinct evidence of bi-modality in the data collected with all three antennas, again suggesting at least two impulsive noise processes. The usefulness of a uni-modal model (generalized extreme value distribution for discone data and Birnbaum-Sanders distribution for the LB horn and HB horn) is therefore doubtful but, of the distributions tried, these were found to be the best fit. Until the reliable identification of distinguishable processes has been achieved there seems little to be gained by seeking more accurate, multimodal distributions to better fit the aggregate process.

The Birnbaum-Saunders distribution is given by:

$$f(t|v,s)=\frac{1}{\sqrt{2\pi}}\left(\frac{\left(\sqrt{\frac{t}{s}}+\sqrt{\frac{s}{t}}\right)}{2vt}\right)\exp\left(-\frac{\left(\sqrt{\frac{t}{s}}-\sqrt{\frac{s}{t}}\right)^2}{2v^2}\right) \quad (5)$$

where v and s are, again, shape and scale parameters. The parameters of both distributions (Birnbaum-Saunders and generalized extreme value) are numerically similar across all three sets of data. That two different distributions have been adopted as best-fit is probably not significant.

Impulse rise-time (Figs. 8(d), 9(d), 10(d) and Table II(B)) also shows some evidence of bi-modality. The t location-scale distribution, i.e.:

$$f(\tau|v,l,s)=\frac{\Gamma\left(\frac{v+1}{2}\right)}{s\sqrt{v\pi}\,\Gamma\left(\frac{v}{2}\right)}\cdot\left[v+\frac{\tau-l}{s}\right]^{-\frac{v+1}{2}} \quad (6)$$

was the best-fit of the distributions tried. The distribution fits the short rise-time data least well and fits the LB horn data less well, generally, than that derived from the other two antennas. Once again we interpret this as indicating the presence of a process in the LB horn data that is absent (or at least present to a lesser extent) in the data from the other antennas. The shape, location and scale parameters of the best-fit curves are, nevertheless, similar for all three antennas.

The exceedance curves of impulse-rate, pulse amplitude, pulse duration and pulse rise-time confirm the distinguishably different behavior of the LB horn data from that of the other two antennas – especially so in the case of impulse rate (Fig. 11) and pulse amplitude (Fig. 12).

Table III contains a summary of the impulsive noise statistics. (The absolute exceedance values for impulse amplitude are not particularly significant since they are partially determined by the arbitrary path-loss from the impulse noise source(s) to the receiving equipment. The relative statistics of impulse rate for the three antennas are, however, significant.) There is an apparent paradox in the rise-time and duration statistics in that the median duration is less than the median rise-time. This is due to the definitions adopted. The rise-time is the conventional 10% - 90% value and the duration is the 3 dB width of the pulse (i.e. the duration between points $1/\sqrt{2}$ times the pulse peak-voltage on either side of the peak.) There is no logical inconsistency, therefore, in the statistics.

The NAD curves in Fig. 16 add to the impression of at least two processes, one of which is more significant in the aggregate signal received by the LB horn than the other two antennas.

VII. Conclusions and Future work

Impulsive noise has been recorded in a 400/275/132 kV electricity substation. The impulsive events have been extracted from raw measurements using a purpose designed de-noising algorithm. A statistical analysis of the de-noised data has been undertaken. There is evidence that at least two distinguishable impulsive processes are present, one of them having a strong periodic or quasi-periodic component. The measurements reported represent aggregated impulsive noise including (potentially) PD, sferic radiation and conventional electromagnetic interference from power-electronics and other equipment.

Impulsive noise models for the assessment of risk associated with the deployment of wireless communications equipment in substations are currently under construction in parallel with the identification of distinguishable processes. Opportunities to make measurements in other substations with a view to assessing substation-to-substation variation are being actively sought in both the UK and Brazil.

References

[1] M. G. Sanchez, I. Cuinas, and A. V. Alejos, "Interference and impairments in radio communication systems due to industrial shot noise," in *Industrial Electronics, 2007. ISIE 2007. IEEE International Symposium on*, 2007, pp. 1849-1854.

[2] M. D. Button, J. G. Gardiner, and I. A. Glover, "Measurement of the impulsive noise environment for satellite-mobile radio systems at 1.5 GHz," *Vehicular Technology, IEEE Transactions on,* vol. 51, pp. 551-560, 2002.

[3] T. K. Blankenship and T. S. Rappaport, "Characteristics of impulsive noise in the 450-MHz band in hospitals and clinics," *Antennas and Propagation, IEEE Transactions on,* vol. 46, pp. 194-203, 1998.

[4] K. L. Blackard, T. S. Rappaport, and C. W. Bostian, "Measurements and models of radio frequency impulsive noise for indoor wireless communications," *Selected Areas in Communications, IEEE Journal on,* vol. 11, pp. 991-1001, 1993.

[5] M. G. Sanchez, L. de Haro, M. C. Ramon, A. Mansilla, C. M. Ortega, and D. Oliver, "Impulsive noise measurements and characterization in a UHF digital TV channel," *Electromagnetic Compatibility, IEEE Transactions on,* vol. 41, pp. 124-136, 1999.

[6] M. G. Sanchez, A. V. Alejos, and I. Cuinas, "Urban wide-band measurement of the UMTS electromagnetic environment," *Vehicular Technology, IEEE Transactions on,* vol. 53, pp. 1014-1022, 2004.

[7] "IEEE Standard for Information technology-Telecommunications and information exchange between systems-Local and metropolitan area networks-Specific requirements - Part 11: Wireless LAN Medium Access Control (MAC) and Physical Layer (PHY) Specifications," *IEEE Std 802.11-2007,* 2007.

[8] Bluetooth SIG, "Specification of the Bluetooth System," 26 July 2007.

[9] "IEEE Standard for Information technology- Telecommunications and information exchange between systems- Local and metropolitan area networks- Specific requirements Part 15.4: Wireless Medium Access Control (MAC) and Physical Layer (PHY) Specifications for Low-Rate Wireless Personal Area Networks (WPANs)," *IEEE Std 802.15.4-2006*, 2006.

[10] M. Hikita, H. Yamashita, T. Hoshino, T. Kato, N. Hayakawa, T. Ueda, and H. Okubo, "Electromagnetic noise spectrum caused by partial

discharge in air at high voltage substations," *Power Delivery, IEEE Transactions on,* vol. 13, pp. 434-439, 1998.
[11] S. Sriram, S. Nitin, K. M. M. Prabhu, and M. J. Bastiaans, "Signal denoising techniques for partial discharge measurements," *Dielectrics and Electrical Insulation, IEEE Transactions on [see also Electrical Insulation, IEEE Transactions on],* vol. 12, pp. 1182-1191, 2005.
[12] L. Satish and B. Nazneen, "Wavelet-based denoising of partial discharge signals buried in excessive noise and interference," *Dielectrics and Electrical Insulation, IEEE Transactions on [see also Electrical Insulation, IEEE Transactions on],* vol. 10, pp. 354-367, 2003.
[13] S. Mallat, *A wavelet tour of signal processing*, 2nd ed. London: Academic Press, 1999.
[14] A. Kyprianou, P. L. Lewin, V. Efthimiou, A. Stavrou, and G. E. Georghiou, "Wavelet packet denoising for online partial discharge detection in cables and its application to experimental field results," *Measurement Science and Technology,* vol. 17, pp. 2367-2379, 2006.
[15] C. S. Chang, J. Jin, C. Chang, T. Hoshino, M. Hanai, and N. Kobayashi, "Separation of corona using wavelet packet transform and neural network for detection of partial discharge in gas-insulated substations," *Power Delivery, IEEE Transactions on,* vol. 20, pp. 1363-1369, 2005.
[16] P. J. Moore, I. Portugues, and I. A. Glover, "A nonintrusive partial discharge measurement system based on RF technology " in *Power Engineering Society General Meeting, 2003, IEEE*, 2003, vol. 2, p. 633.
[17] I. E. Portugues, P. J. Moore, and I. A. Glover, "An investigation into the effect of receiver bandwidth for the interpretation of partial discharge impulses using remote radio sensing," in *International University Power Engineering Conference*, 2002, pp. 529-533.
[18] Q. Shan, I. A. Glover, P. J. Moore, I. E. Portugues, M. Judd, R. Rutherford, and R. J. Watson, "TEM horn antenna for detection of impulsive noise," in *EMC Europe 2008*, Hamburg, Germany, 2008.
[19] I. Portugues, P. J. Moore, I. A. Glover, C Johnstone, R H McKosky, M B Goff and L V Zel, "RF-based partial discharge early warning system for air-insulated substations " *IEEE Transactions on Power Delivery, Vol. 24 No. 1, 2009,* pp.20-29.
[20] Q. Shan, S. Bhatti, I. A. Glover, R. Atkinson, I. E. Portugues, P. J. Moore, and R. Rutherford, "Extraction of impulsive noise from measurements in a 400 kV electricity substation," *Proceedings of the 4th IASME/WSEAS International Conference on Energy and Environment,* Cambridge, UK, 2009, pp. 135-139.
[21] M. Evans, N. Hastings and B. Peacock, "Statistical Distributions", Wiley-Interscience, 3rd Edition, ISBN-10: 0471371246, Chap. 5, pp. 34-42.
[22] Z.W. Birnbaum and S.C. Saunders, "A New Family of Life Distributions", *Applied Probability Trust, Vol. 6, No. 2, August 1969*, pp. 319-327.
[23] M. Evans, N. Hastings and B. Peacock, "Statistical Distributions", Wiley-Interscience, 3rd Edition, ISBN-10: 0471371246, Chap. 16, pp. 85-89.
[24] J. F. Lawless, "Statistical Models and Methods for Lifetime Data", Wiley Series in Probability and Statistics, Wiley-Blackwell, 2nd Edition, ISBN-10**:** 0471372153, Sec 5.2, p215.
[25] M. Evans, N. Hastings and B. Peacock, "Statistical Distributions", Wiley-Interscience, 3rd Edition, ISBN-10: 0471371246, Chap. 31, pp. 151-154.
[26] J. F. Lawless, "Statistical Models and Methods for Lifetime Data", Wiley Series in Probability and Statistics, Wiley-Blackwell, 2nd Edition, ISBN-10**:** 0471372153, Sec 4.2.2, p 170.
[27] J. F. Lawless, "Statistical Models and Methods for Lifetime Data", Wiley Series in Probability and Statistics, Wiley-Blackwell, 2nd Edition, ISBN-10**:** 0471372153, Sec. 1.3.4, p 23.
[28] M. Evans, N. Hastings and B. Peacock, "Statistical Distributions", Wiley-Interscience, 3rd Edition, ISBN-10: 0471371246, Chap. 25, pp. 124-128.
[29] M. Nakagami, "The m-distribution - A general formula of intensity distribution of rapid fading, in Statistical Methods in Radio Wave Propagation," W. C. Hoffman, Ed. Elmsford, NY: Pergamon, 1960.
[30] M. Evans, N. Hastings and B. Peacock, "Statistical Distributions", Wiley-Interscience, 3rd Edition, ISBN-10: 0471371246, Chap. 42, pp. 192-203.
[31] S. Oranc, "Ignition noise measurements in the VHF/UHF bands," *IEEE Trans. Electromagn. Compat., vol EMC-17,* pp. 135-139, May 1975.

Qingshan Shan (M'04) graduated with PhD degree in system engineering from Nottingham Trent University (UK) in 2004.

He was a Research Assistant with the University of Portsmouth (UK) from 2003 to 2005, a Research Officer with University of Bath (UK) from 2005 to 2006 and a Research Fellow with University of Strathclyde (Glasgow, UK) from 2007 to 2009. His research involved in the areas of wireless communications, ground penetrating radar, digital signal processing and artificial intelligence applications. Currently he is a Software Development and Electronics Engineer with the MRC Institute of Hearing Research (Nottingham, UK).

Ian A. Glover (M'90) graduated with a BEng degree in electronic and electrical engineering from the University of Bradford (UK) in 1981 and with a PhD degree in radio science from the same University in 1987.

He started his career as a trainee technician (and later professional) engineer at the Yorkshire Electricity Board, became a Lecturer in Electrical and Electronic Engineering at the University of Bradford in 1984 and later Senior Lecturer in Telecommunications, also at the University of Bradford. From 1999 to 2006 he was Senior Lecturer in Telecommunications at the University of Bath (UK) and from 2006 he has been Reader in Radio Science & Wireless Communications at the University of Strathclyde (UK). He is currently CAPES Visiting Professor at the Federal Universidade de Campina Grande (2009 to 2010). He is the author with P M Grant of Digital Communications, Pearson Prentice-Hall (1998, 2004, 2010), which is now in its third edition. He is also editor, with P R Shepherd and Steve R Pennock of Microwave Devices, Circuits and Subsystems for Communications Engineering, Wiley, 2005. His research interests are in radio propagation, interference and noise.

Dr. Glover is a member of the Institution of Engineering and Technology (IET), a fellow of the Higher Education Academy and is the UK Member of Commission E (Electromagnetic Interference and Noise) of the International Union of Radio Science.

Robert Atkinson (M'97–SM'07) graduated with a BEng (Hons) degree in electronic and electrical engineering from the University of Strathclyde in 1993; he subsequently obtained an MSc in communications, control and digital signal processing in 1996 and a PhD in mobile communications systems in 2003 from the same university. He became a member of the IEEE in 1997 and a senior member in 2007.

He has worked in the University of Strathclyde since 1997 as a Research Assistant, a Research Fellow, a Senior Research Fellow, and currently as a Lecturer.

Dr Atkinson is a member of the Institution of Engineering and Technology and a Fellow of the Higher Education Academy.

Shahzad A. Bhatti (M'05) - was born in M.B-Din, Pakistan on October 19, 1981 and is currently pursuing his PhD degree (2007 to 2010) in electrical and electronic engineering at University of Strathclyde (UK). He received his BSc in computer engineering (with Honours) from University of Engineering and Technology Taxila (Pakistan) in 2005 and MSc in mobile and satellite communications from University of Surrey (UK) in 2007.

He worked as Lecturer in Computer and Software Engineering at University of Engineering and Technology Taxila (Pakistan) from January 2005 to August 2006. His research interests include wireless transceiver design for industrial environments, impulsive noise modelling and digital signal processing.

Iliana E. Portugues (M'03) was born in Madrid, Spain, in 1979. She received the M.Eng. degree in electronic and communication engineering and the Ph.D. degree in radiometric equipment diagnostics from the University of Bath, Bath, U.K., in 2001 and 2004, respectively.

From 2001 to 2005, she was a Research Officer with the University of Bath. From 2005 to 2007, she was a Research Fellow in the Institute for Energy and Environment with the University of Strathclyde, investigating characteristic RF emissions from defective substation insulation. She is a Founder and Director of Elimpus Ltd., Bellshill, U.K.

Philip J. Moore (SM'96) was born in Liverpool, U.K., in 1960. He received the B.Eng. degree in electrical engineering from Imperial College, London, U.K., in 1984 and Ph.D degree in power system protection from City University, London, in 1989.

From 1984 to 1987, he was a Development Engineer with GEC Measurements. He began his academic career at City University in 1987, and was with the University of Bath, Bath, U.K., from 1991 to 2005. Currently, he is a professor of Electrical Plant and Diagnostics in the Institute for Energy and Environment, University of Strathclyde, U.K. His research interests include radio-frequency emissions from power system equipment, harmonics,

numeric protection, high-voltage discharges, power system simulation, and fault location.

Prof Moore is a Charted Engineer in the U.K. He is a Founder and Director of Elimpus Ltd., Bellshill, U.K.

Maria de Fátima Queiroz Vieira received her Degree in Physics from the UFPE, Brazil, in 1975, her Master degree in Electrical Engineering in 1979 from UFPB, Brazil; and a PhD in Electrical Engineering from Bradford University, in the UK, in 1986. She is a senior lecturer at the Electrical Engineering Department of UFCG, in Brazil, where she works since 1977, both in the undergraduate and graduate levels. She is currently the head of the Man Machine Interface Laboratory (LIHM) at UFCG.

Antonio Marcus N. Lima (M'77-SM'05) was born in Recife, Pernambuco, Brazil, in 1958. He received the Bachelor's and Master's degrees in electrical engineering from Universidade Federal da Paraíba - UFPB, Campina Grande, Paraíba, Brazil in 1982 and 1985, respectively. He received his doctoral degree in electrical engineering in 1989 from Institut National Polytechnique de Toulouse - INPT, Toulouse, France. He was with the Escola Técnica Redentorista - ETER, Campina Grande, Paraíba, Brazil from 1977 to 1982 and was a Project Engineer at Sul-América Philips, Recife, Pernambuco, Brazil, from 1982 to 1983. From 1983 to March 2002 he was with the Electrical Engineering Department of UFPB where he became Full Professor in 1996. At UFPB he was Coordinator of Graduate Studies from 1991 to 1993 and from 1997 to 2002. Since April 2002 he has been with the Department of Electrical Engineering of the Universidade Federal de Campina Grande where he is currently Full Professor and Head of the Department of Electrical Engineering. His current research interests are in the fields of electrical machines and drive systems, industrial automation, embedded systems, electronic instrumentation, control systems and system identification.

Benemar Alencar de Souza (M'02–SM'05) received his bachelor, master and doctoral degrees in Electrical Engineering from Federal University of Paraíba (UFPB), Campina Grande, Brazil, in 1977, 1981 and 1995, respectively. He is currently an associated professor of the Electrical Engineering Department at Federal University of Campina Grande (UFCG), Campina Grande, Brazil.

Dr Souza's research activities are focused on optimization methods and meta-heuristics applied to power systems planning and automation, distributed generation, electromagnetic transients and digital protection.

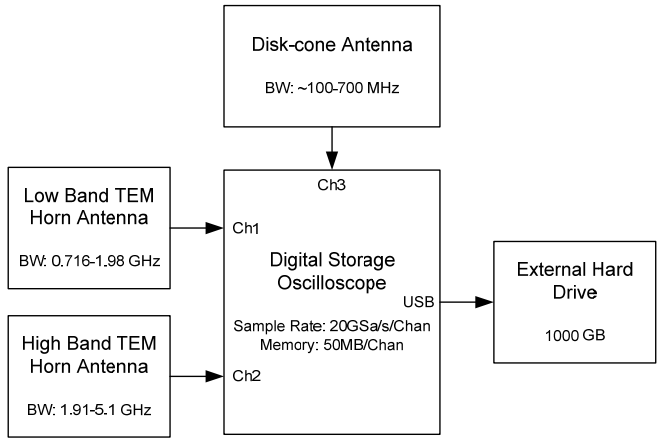

Figure 1 Impulsive noise detection and recording system

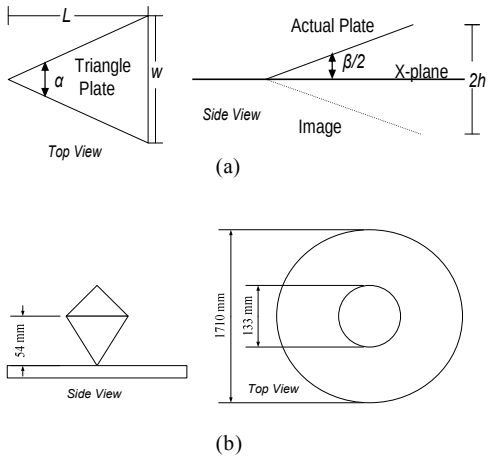

Figure 2: Schematic diagrams of antennas: (a) TEM horn and (b) discone antenna

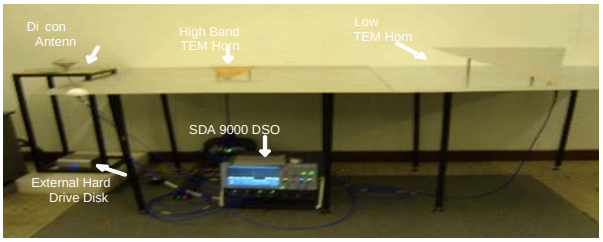

(a)

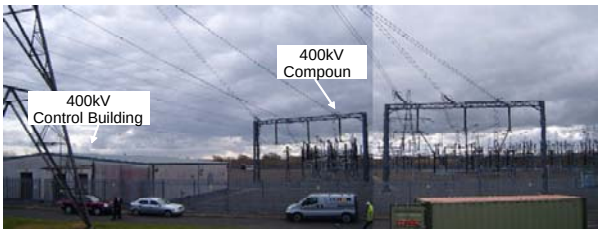

(b)

(c)

(d)

Figure 3: Measurement system and site: (a) impulsive noise detection and recording system deployed in substation control room, and Strathaven substation, (b) 400 kV compound, (c) 275 kV compound, and (d) 132 kV compound.

Figure 4: Location of measurement equipment (A) 400 kV control room, (B) 275 kV control room

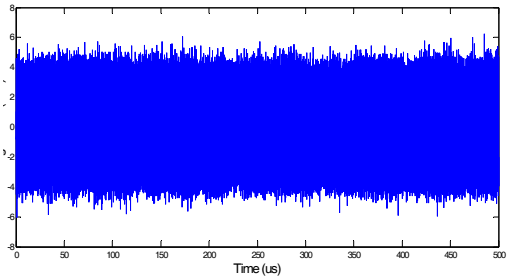

(a)

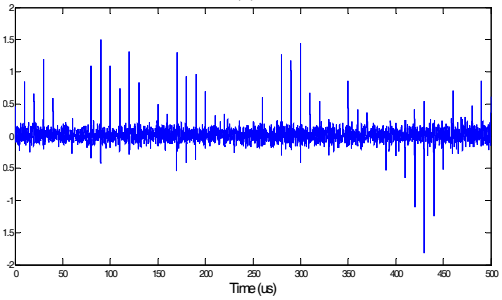

(b)

Figure 5: Raw and de-noised data (mV): (a) raw measurement and (b) de-noised impulses.

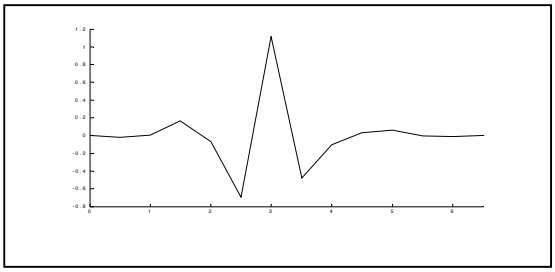

Figure 6: Symlet-6 wavelet

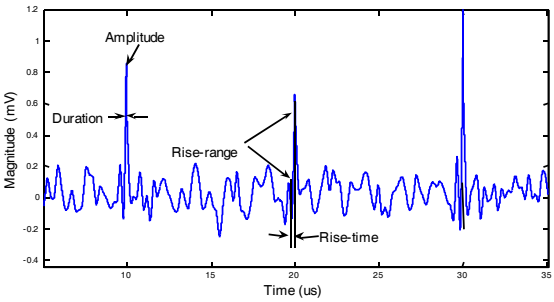

Figure 7: Illustration of impulse features: amplitude, duration, and rise-time.

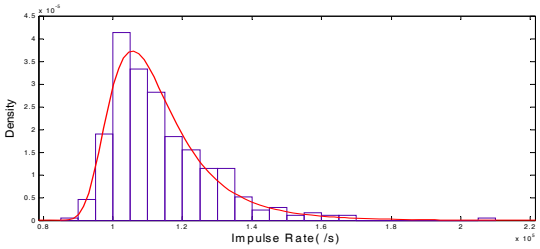

(a)

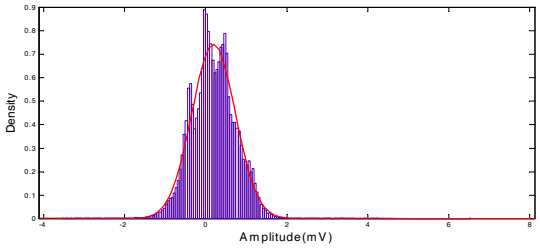

(b)

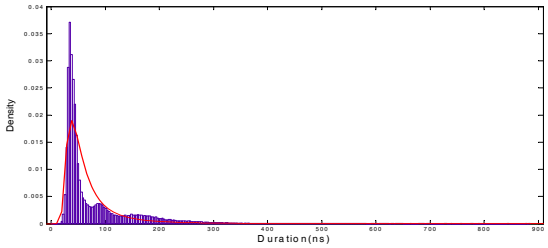

(c)

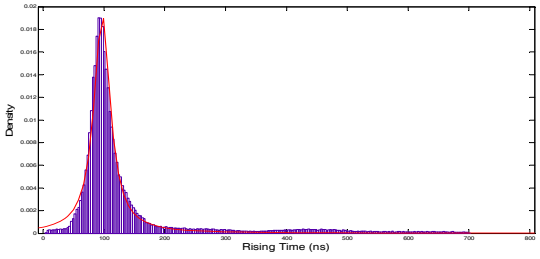

(d)

Figure 8: PDFs for discone: (a) mean impulse rate, (b) impulse amplitude, (c) impulse duration, and (d) impulse rise-time

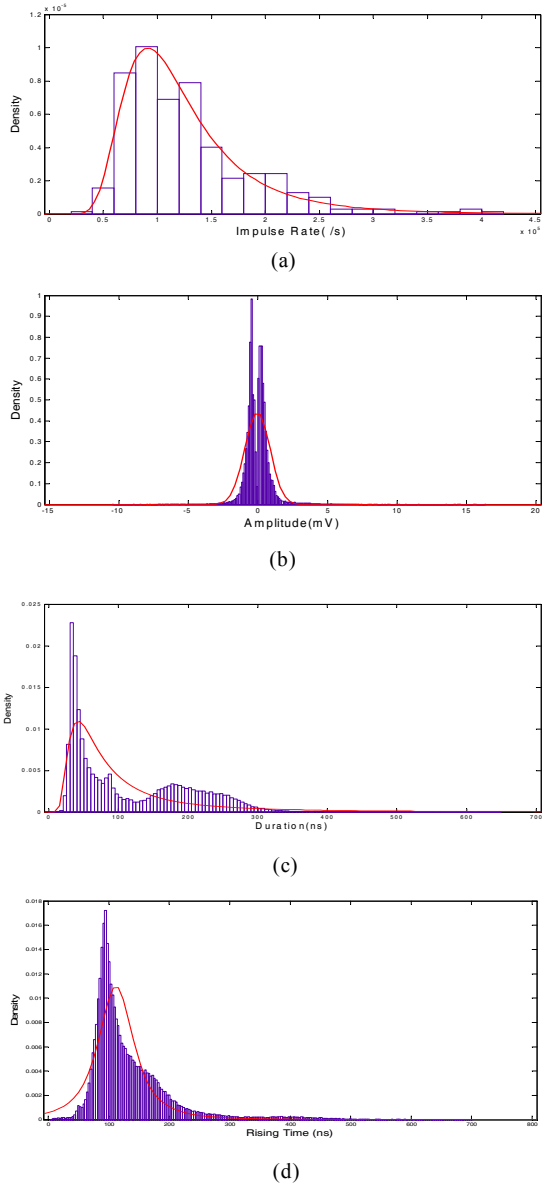

Figure 9: PDFs for LB horn: (a) mean impulse rate, (b) impulse amplitude, (c) impulse duration, and (d) impulse rise-time

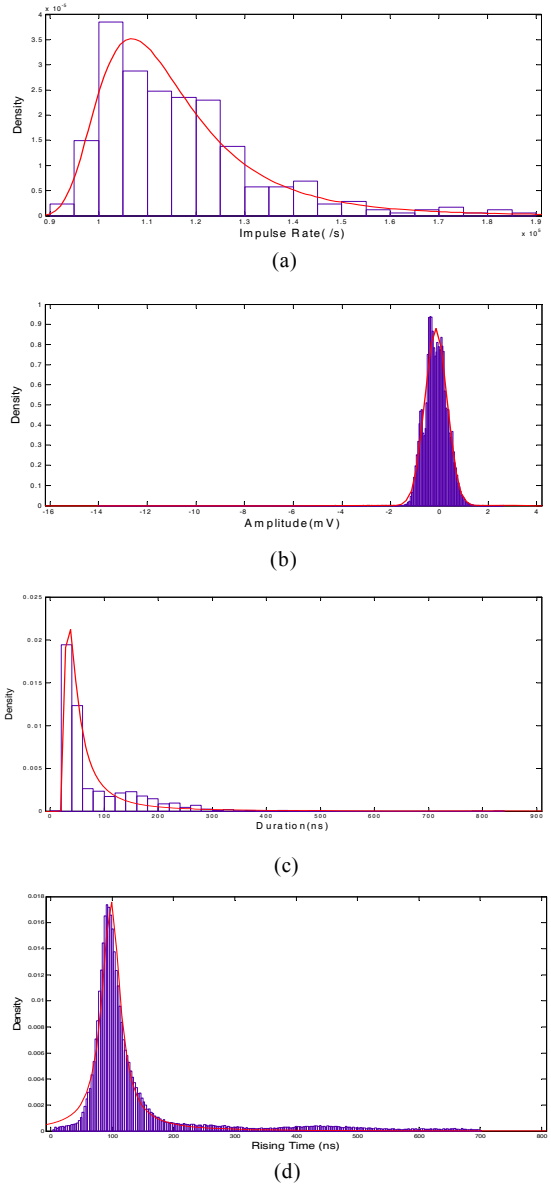

Figure 10: PDFs for HB horn: (a) mean impulse rate, (b) impulse amplitude, (c) impulse duration, and (d) impulse rise-time

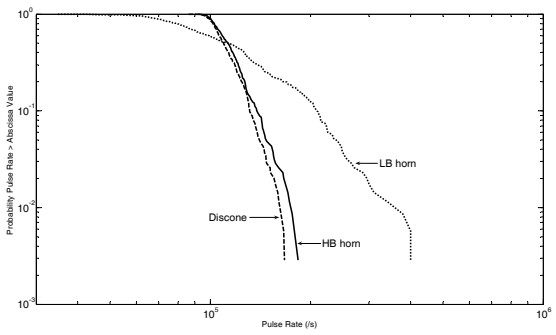

Figure 11: Exceedance curves of impulse rate for discone, LB horn and HB horn

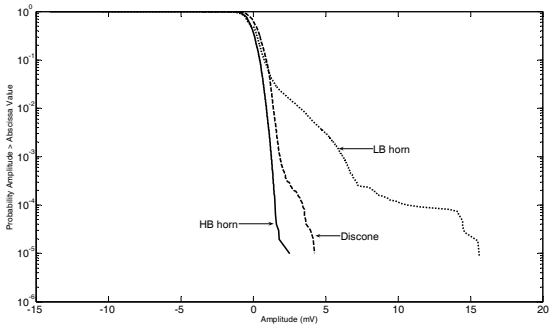

Figure 12: Exceedance curves of pulse amplitude for discone, LB horn and HB horn

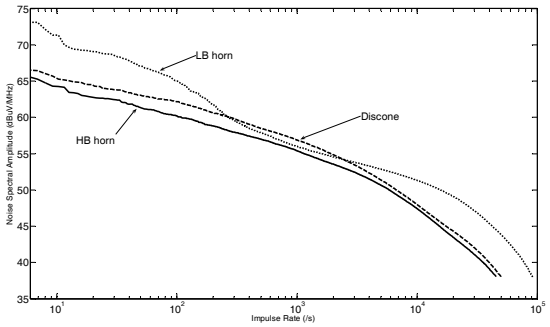

Figure 16: NAD curves for discone, LB horn and HB horn

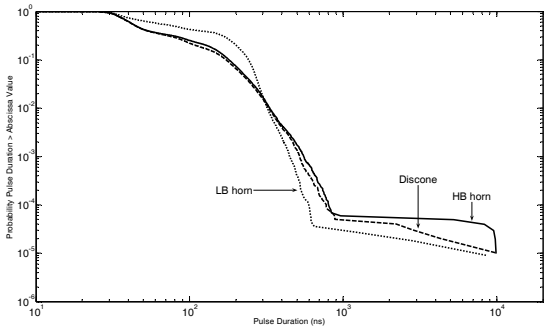

Figure 13: Exceedance curves of pulse duration for discone, LB horn and HB horn

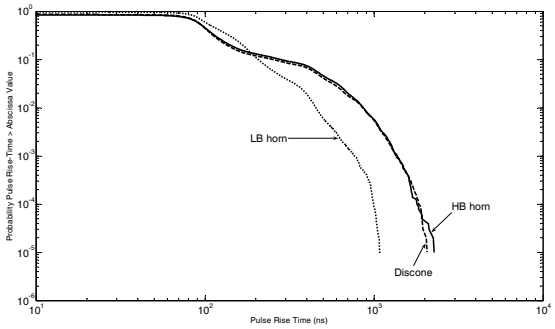

Figure 14: Exceedance curves of pulse rise-time for discone, LB horn and HB horn

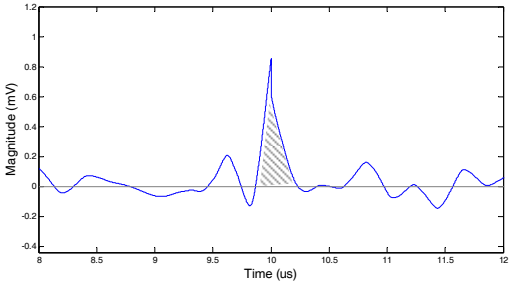

Figure 15: Definition of 'impulse' strength (shaded region)